SELF-ALIGNED FABRICATION AND CONTACT LINE PINNING CHARACTERIZATION OF PEDESTAL NOZZLES

Bjorn T.H. Borgelink[*], Erwin J.W. Berenschot, Remco G.P. Sanders, Stefan Schlautmann, Han Gardeniers[*], Niels R. Tas[*]

University of Twente, Faculty of Science and Technology, Mesoscale Chemical Systems group, THE NETHERLANDS

2022 IEEE 35th International Conference on Micro Electro Mechanical Systems Conference (MEMS) | 978-1-6654-0911-7/22/$31.00 ©2022 IEEE | DOI: 10.1109/MEMS51670.2022.9699536

ABSTRACT

Silicon dioxide pedestal nozzles are introduced, featuring a sharp concentric rim with an edge angle of approximately 5° and a sub-20 nm radius of curvature. The nozzles show an unprecedented ability to pin the contact line of de-ionized water, and apparent contact angles exceeding 210° were observed. A dynamic contact angle characterization method is introduced to determine the pinning capabilities of the nozzle. The nozzle is vibrated with a piezo actuator and brings pendant droplets close to their resonance frequency. Larger contact angles are observed for smaller droplets, because they can be driven closer to the resonance frequency before pinch-off.

KEYWORDS

Micronozzle, silicon machining, microfluidics, droplet, contact line pinning

INTRODUCTION

In many microfluidic applications, such as inkjet printing [1], electrospinning [2], electrospraying [3,4], pendant droplet tensiometry [5] and monodisperse emulsion fabrication [6], a liquid adheres to a microfluidic nozzle. For these applications it is desired that the contact area of the liquid on the nozzle is fixed.

A common strategy to confine (and thereby control) the liquid contact area is to either use an anti-wetting material outside the periphery of the contact area [4] or employ geometrical features to pin the three-phase contact line [3,5]. Depending on the application, the use of anti-wetting materials has practical limitations, such as ageing, surface pollution and resistance to heat and chemicals [1]. Furthermore, if the dimensions of the nozzle are scaled down, applying an anti-wetting layer with the required accuracy is difficult. Depending on the nozzle fabrication method, including a sharp geometrical discontinuity in the nozzle design to induce contact line pinning [7] is more feasible. If the geometrical discontinuity is defined with higher accuracy, the pinning effect improves [7].

Micro-nozzles made of anti-wetting materials [4] and with geometrical discontinuities [3,5] reported in literature have been fabricated with processes that allow a limited feature size resolution. Hence, the contact line pinning effect is expected not to be strong. Furthermore, nozzles made solely from an anti-wetting material do not provide a strong adhesion to polar liquids.

Our approach is to employ a self-aligned microfabrication strategy for the wafer-scale fabrication of sharp-edged silicon dioxide pedestal nozzles [8]. The nozzle consists of a tube with a concentric rim at the tube end, which both are protruding a silicon surface (Figure 1). Because the nozzle is made of silicon dioxide, polar liquids adhere strongly to the nozzle.

The essential feature of the nozzle is the rim edge, which has approximately a 5° angle and a sub-20 nm radius of curvature. According to Gibbs' inequality, the range of achievable apparent contact angles θ at mathematically sharp corners is calculated as:

$$\theta_0 \leq \theta \leq 180° - \varphi + \theta_0 \quad (1)$$

where φ is the rim edge angle and θ_0 the macroscopic equilibrium contact angle of the liquid on a flat (silicon dioxide) surface [7]. Assuming that the nozzle rim edge is sufficiently sharp such that Equation 1 can be employed and using $\varphi \approx 5°$, the apparent contact angle of droplets pinned on the nozzle rim can be increased with approximately 175°.

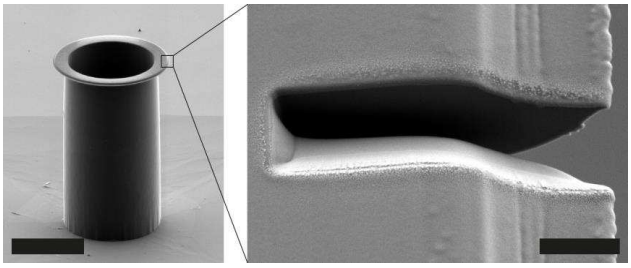

Figure 1: SEM images of the obtained nozzle feature (left) and cross-section of the nozzle rim showing the sharpness of the rim edge (right). The rim is covered with platinum prior to milling the cross-section cut. Scale bar sizes left and right are 50 µm and 900 nm.

In a preliminary characterization, the size of droplets pinned on the nozzle was controlled by a constant applied pressure. This process has an intrinsic instability at 90° apparent contact angle, after which uncontrolled droplet growth occurs [8]. Image analysis of sessile de-ionized water (DI-water) droplets pinned on the nozzle have revealed that the pinned macroscopic contact angle exceeds 180° [8]. However, accurate contact angle measurements are difficult due to the uncontrolled nature of the process.

To better characterize the nozzle's potential to pin the contact line, a novel dynamic contact angle measuring technique has therefore been developed. The technique, using droplet vibration close to its resonance frequency, allows for measuring contact angles exceeding 180°.

In this paper, after summarizing the main nozzle fabrication steps, the novel dynamic contact angle measuring technique is described, followed by presenting and discussing the measuring results that were obtained by analyzing DI-water droplets pending on a nozzle with 36 µm rim radius.

EXPERIMENTAL METHODS

Pedestal nozzle fabrication

The main nozzle microfabrication process steps are schematically depicted in Figure 2. Details about the fabrication process are discussed in [8].

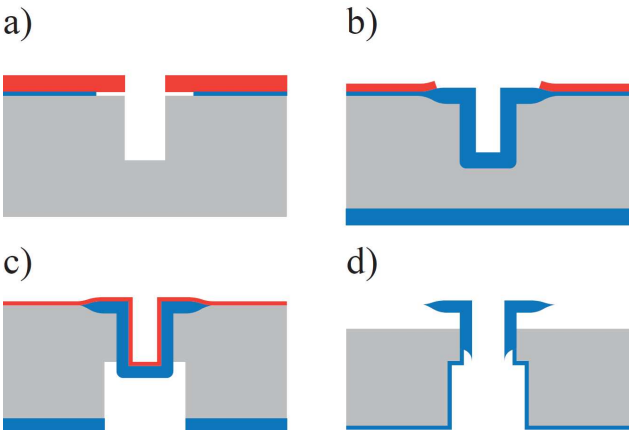

Figure 2: a-d) Drawings of the nozzle fabrication process at essential stages. a) Definition of the nozzle rim by sacrificial etching of the silicon dioxide (blue) under the silicon nitride mask (red). b) Fabricating the nozzle feature by means of local oxidation of silicon (LOCOS). c) Removing the silicon nitride remnants and depositing a new thin silicon nitride hard mask, etching the silicon dioxide and silicon at the back side of the substrate. d) Liberating the nozzle feature by etching the silicon substrate (gray).

Circular holes are etched in the layer stack and underlying silicon by means of (deep) reactive ion etching. With an aqueous HF solution, the silicon dioxide underneath the silicon nitride layer is selectively and isotropically etched (Figure 2a). This etching technique in which edges of the mask is used to allocate the starting point at which the sacrificial layer starts to etch, is referred to as edge lithography [9]. Subsequently, the silicon nitride is selectively etched in aqueous phosphoric acid. This timed etch step is stopped once the suspended part of the layer is removed and leaves a thinner silicon nitride layer on top of the silicon dioxide. The edge lithography-based etching process concentrically retracts the layer stack from the silicon hole and determines the size of the nozzle rim.

Silicon not masked by the silicon nitride is converted into silicon dioxide during the LOCOS. During this step, the nozzle tube and rim are formed (Figure 2b). Thanks to the well-known birds' beak effect occurring during the LOCOS [10], the nozzle rim gets the sharp and well-defined edge.

A second etching method is applied to selectively open the silicon dioxide blind hole and facilitate a fluidic connection to the back side of the substrate. The silicon nitride hard mask and thin silicon dioxide layer on the front side of the substrate is removed, and a thinner silicon nitride hard mask is deposited. With (deep) reactive ion etching, holes are etched in the silicon dioxide and silicon at the back side of the substrate (Figure 2c). The process to etch the silicon does not etch the silicon dioxide, which acts as a buried etch stop layer.

With aqueous HF the uncovered silicon dioxide is etched, thereby opening the blind hole. A second LOCOS is employed to grow a thin silicon dioxide layer on the bare silicon and protects silicon against subsequent wet chemical etchants. The silicon nitride is removed in aqueous phosphoric acid, and the unprotected silicon is selectively etched in aqueous tetramethylammonium hydroxide (Figure d).

Dynamic contact angle measurements

A schematic drawing of the measuring setup is shown in Figure 3.

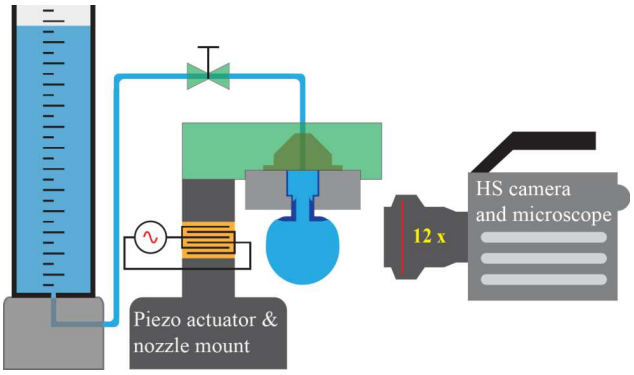

Figure 3: Schematic drawing of the dynamic measuring system. A gravity-directed liquid column is connected to the microfluidic nozzle via a shut off valve. The nozzle is mounted on a piezo actuator, which vibrates along the axis of gravity with a fixed amplitude and frequency controlled by a function generator. A high-speed (HS) camera equipped with a microscope system is used to capture pictures of the droplet adhering to the nozzle. A light source (not depicted in the figure) illuminates the droplet on the opposite site of the camera.

Nozzles are mounted on a home-built holder, which connects the nozzle to the fluid column and allows the nozzle to be mounted on the piezo actuator (Physik Instrumente). The height of the liquid column as well as the position of the shut off valve can be varied to change the fluid flow supplied to the nozzle. A signal generator (Agilent 33210a) and a signal amplifier (Physik Instrumente) are used to drive the piezo with a fixed amplitude and frequency. The nozzle is directed along gravity and moves parallel to the axis of gravity. A home-built high-power light source based on a LED light panel (Luminous Devices CVM-32-56-95-54-AC00-F2-3) is used to illuminate the droplet and nozzle with mainly visible light. DI-water does not adsorb the light emitted by the light source, and radiative heating of the liquid by light is not expected to occur. A high-speed camera (Photron Fastcam SA-X2) equipped with a Navitar 12x zoom lens system is used to capture the nozzle and droplet with 2000 frames per second. A MATLAB script developed to automatically determine the position of the droplet interface and walls of the nozzle is used to analyze the obtained images. The resolution of the system is between 1.8 µm and 1.95 µm/pixel.

The strategy for measuring pinned contact angles larger than 180° is to drive the droplet close to its resonance frequency, such that for a small nozzle amplitude the oscillatory droplet displacement is large. While the nozzle oscillates, a flow through the nozzle

increases the droplet volume and, thus, its mass. Once the droplet mass approaches the mass at which it resonates, its amplitude rapidly increases. Before the droplet resonates, the amplitude of the oscillating motion grows so large that necking of the liquid meniscus occurs and the droplet detaches from the nozzle.

The periodic motion of the nozzle rim is tracked in time if $\theta < 180°$. In this case, the droplet does not block the view on the nozzle rim. Otherwise, the position of the rim edge is predicted by fitting the available data with an oscillating function. The position of the liquid-vapor interface of the droplet is also traced in each image, and if $\theta > 180°$ the highest point on this interface is determined. A geometrical relation (Figure 4) then allows the calculation of the lower limit of the apparent contact angle.

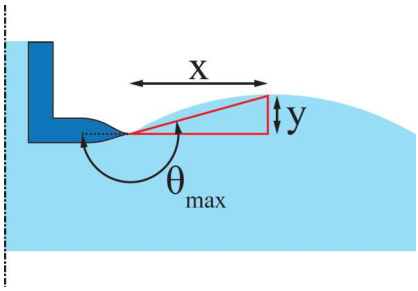

Figure 4: A liquid droplet (light blue) adhering to the nozzle tube (dark blue). The highest point on the droplet interface is a horizontal distance x and a vertical distance y separated from the nozzle rim edge. θ_{max} indicates the lower limit of the maximum apparent contact angle.

Choosing the rim edge to be at the origin, the highest point on the interface has coordinates (x,y). In this case, the lower limit of the maximum contact angle θ_{max} is calculated as:

$$\theta_{max} = 180° + \tan^{-1}(y/x) \qquad (2)$$

EXPERIMENTAL RESULTS

Dynamic contact angle measurements

Figure 5 shows a series of images that were obtained during one of the dynamic contact angle measurements.

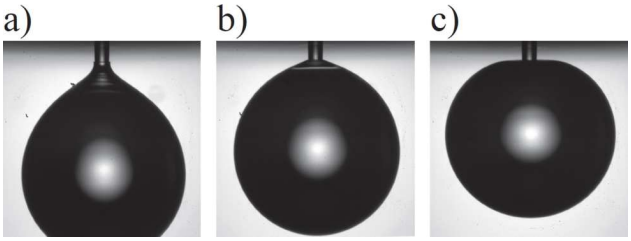

Figure 5: Images taken in successive order of a DI-water droplet pending on the vibrating nozzle with a tube radius of 27 µm. The droplet oscillates at a frequency close to its resonance frequency. In a), the center of mass of the droplet is at its lowest point and the contact angle is close to 90°, whereas in c) the center of mass is at its highest point and the contact angle is larger than 180°.

With a conventional sessile drop measuring system (Dataphysics OCA-20), the equilibrium contact angle of DI-water on silicon dioxide was measured to be $\theta_0 = 34 \pm 6°$ [8]. Although the apparent contact angle of vibrating droplets can be smaller than 90° if necking of the liquid meniscus occurs (Figure 5a), it still is larger than the equilibrium contact angle. Hence, the contact line does not recess, and droplet detachment is only caused by necking of the liquid interface. Inferred from Equation 1, the maximum apparent contact angle of DI-water is $\theta = 209 \pm 6°$.

In Figure 6 the measured apparent contact angle of a pinned droplet is plotted as a function of time.

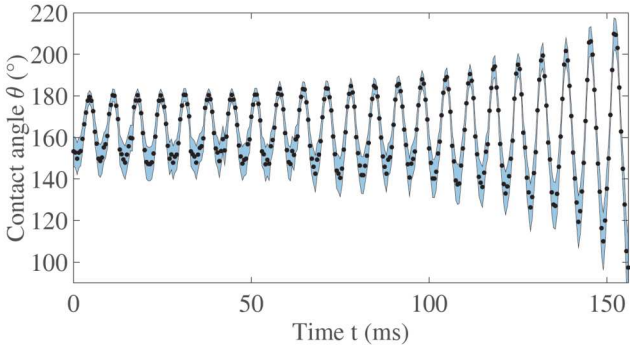

Figure 6: The measured contact angle θ plotted in time. The nozzle oscillates at a frequency of 150 Hz. The blue band around the black data points denote the measuring error.

Prior to detachment of the droplet occurring at $t \approx 156$ ms, it has an average horizontal diameter of 690 ± 10 µm. Initially, the maximum apparent contact angle is approximately 180° but quickly increases to $\theta_{max} = 212 \pm 8°$ prior to its detachment. Considering the measuring error, the maximum apparent contact angle is smaller than the maximum apparent contact angle predicted by Gibbs' inequality (Equation 1).

Maximum contact angle vs. nozzle frequency

Figure 7 shows the maximum apparent contact angle θ_{max} measured for different nozzle frequencies f. For all measurements, the amplitude of the oscillating nozzle is 4.1 ± 0.2 µm. These maximum apparent contact angles were measured right before the droplet starts to resonate.

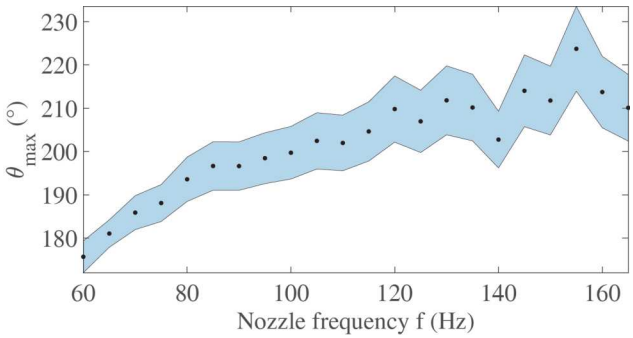

Figure 7: The measured maximum apparent contact angles θ_{max} as a function of the nozzle frequency f. The blue band around the black data points denote the measuring error.

The data points at f = 140 Hz and f = 155 Hz deviate within error from the global trend of θ_{max} vs. f. These deviations are caused by reflections of light at the droplet interface close to the nozzle, which are also observed in

Figure 5b.

For lower nozzle frequencies and for larger droplet sizes, θ_{max} is smaller than for higher frequencies and smaller droplets. To understand this phenomenon, the lowest point of the droplet interface is tracked in time. The results obtained for two different nozzle frequencies f are plotted in Figure 8.

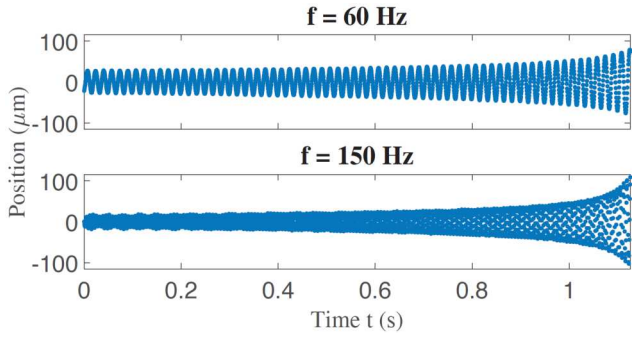

Figure 8: The position of the lowest point of an oscillating droplet's interface plotted as a function of time. The measuring error is estimated to be ± 2 μm. A zero position belongs to the equilibrium position of the oscillation. At t ≈ 1.13 s, the droplets detach.

At t = 0 s, the amplitude of droplet oscillating at 60 Hz is larger than the smaller droplet oscillating at 150 Hz, because larger droplets deform more compared to small droplets. However, before the droplets are detaching at t ≈ 1.13 s, the amplitude of the droplet oscillating at 150 Hz is larger compared to the larger and easier-to-deform droplet oscillating at 60 Hz. These observations as well as phase measurements, suggest that smaller droplets can be driven closer to their resonance frequency than larger droplets, because larger droplets detach well before resonance occurs.

CONCLUSION

The main microfabrication steps for silicon dioxide pedestal nozzles are summarized. The vital part for confining the contact area of liquids to the nozzle, is the nozzle rim with a sharp edge that has approximately a 5° angle and a sub-20 nm radius of curvature.

A novel dynamic contact angle measuring technique is presented, based on vibrating the pedestal nozzle with a fixed frequency along the axis of gravity, while a liquid droplet adhering to the nozzle rim is slowly growing and oscillates at the same frequency as the nozzle. This dynamic contact angle strategy was successfully used to measure apparent contact angles larger than 180°.

DI-water droplets with apparent contact angles exceeding 210° have been measured, which is of the same order as the maximum apparent contact angle predicted by Gibbs' theory [7]. The largest apparent contact angles are measured right before the droplet detaches from the nozzle, which is caused by necking of the liquid meniscus. Furthermore, the largest apparent contact angles were measured for the smallest droplets and highest oscillation frequencies. This is because forces acting on larger droplets cause severe necking and detach from the nozzle well before they start to resonate.

Larger microscope magnifications and optimization of the illumination are necessary to determine the lower limit of the maximum apparent contact angle θ_{max} with greater accuracy.

ACKNOWLEDGEMENTS

B.T.H.B. highly appreciated the help of Jelle Schoppink with setting up the high-speed camera. B.T.H.B., E.J.W.B., H.G. and N.R.T received funding from the European Research Council (ERC) under the European Union's Horizon 2020 research and innovation program (grant agreement no. 742004).

REFERENCES

[1] J. de Jong, H. Reinten, H. Wijshoff, M. van den Berg, K. Delescen, R. van Dongen, F. Mugele, M. Versluis, D. Lohse, "Marangoni flow on an inkjet nozzle plate", *Appl. Phys. Lett.*, vol. 91, pp. 204102, 2007.

[2] D. H. Reneker, I. Chun, "Nanometre diameter fibres of polymer, produced by electrospinning", *Nanotechnology*, vol. 7, pp. 216-223, 1996.

[3] S. Arscott, S. Le Gac, C. Druon, P. Tabourier, C. Rolando, "A micro-nib nanoelectrospray source for mass spectrometry", *Sens. Actuators B: Chem.*, vol. 98, pp. 140-147, 2004.

[4] L. Licklider, X.-Q. Wang, A. Desai, Y.-C. Tai, T. D. Lee, "A Micromachined Chip-Based Electrospray Source for Mass Spectrometry", *Anal. Chem.*, vol. 72, pp. 367-375, 2000.

[5] L. M. Y. Yu, J. J. Lu, Y. W. Chan, A. Ng, L. Zhang, M. Hoorfar, Z. Policova, K. Grundke, A. W. Neumann, "Constrained sessile drop as a new configuration to measure low surface tension in lung surfactant systems", *J. Appl. Physiol.*, vol. 97, pp. 704-715, 2004.

[6] C. Berkland, K. K. Kim, D. W. Pack, "Fabrication of PLG microspheres with precisely controlled and monodisperse size distributions", *J. Control. Release.*, vol. 73, pp. 59-74, 2001.

[7] J. F. Oliver, C. Huh, S. G. Mason, "Resistance to spreading of liquids by sharp edges", J. Colloid Interface Sci., vol. 59, pp. 568- 581, 1977.

[8] B. T. H. Borgelink, E. J. W. Berenschot, R. G. P. Sanders, S. Schlautmann, N. R. Tas, J. G. E. Gardeniers, "Fabrication and characterization of microfluidic pedestal nozzles enabling geometric contact line pinning", submitted to *Lab on a Chip*.

[9] Y. Zhao, E. Berenschot, H. Jansen, N. Tas, J. Huskens, M. Elwenspoek, "Multi-silicon ridge nanofabrication by repeated edge lithography", *Nanotechnology*, vol. 20, pp. 315305, 2009.

[10] T.-C. Wu, W. T. Stacy, K. N. Ritz, "The influence of the LOCOS processing parameters on the shape of the bird's beak structure", J. electrochem. Soc., vol. 130, pp. 1563-1566, 1983.

CONTACT

*B. T. H. Borgelink, b.t.h.borgelink@utwente.nl
*H. Gardeniers, j.g.e.gardeniers@utwente.nl
*N. R. Tas, n.r.tas@utwente.nl